

Predicting Order and Disorder for β -Peptide Foldamers in Water

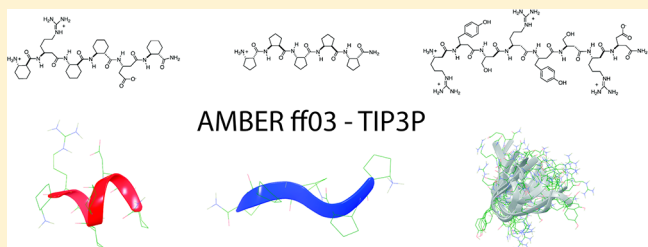
Lukács J. Németh,[†] Zsófia Hegedüs,[†] and Tamás A. Martinek*,^{†,‡}

[†]SZTE-MTA Lendulet Foldamer Research Group, Institute of Pharmaceutical Analysis, University of Szeged, Somogyi u. 6, H-6720 Szeged, Hungary

[‡]Institute of Pharmaceutical Chemistry, University of Szeged, Eötvös u. 6, H-6720 Szeged, Hungary

Supporting Information

ABSTRACT: Following a quantitative validation approach, we tested the AMBER ff03 and GAFF force fields with the TIP3P explicit water model in molecular dynamic simulations of β -peptide foldamers. The test sequences were selected to represent a wide range of folding behavior in water: compact helix, strand mimetic geometry, and the state of disorder. The combination AMBER ff03–TIP3P successfully predicted the experimentally observed conformational properties and reproduced the NOE distances and backbone 3J coupling data at a good level. GAFF was unable to produce folded structures correctly due to its biased torsion potentials. We can recommend AMBER ff03–TIP3P for simulations involving β -peptide sequences in aqueous media including ordered and disordered structures.



INTRODUCTION

Peptidic foldamers constructed by using β -amino acid building blocks are close analogs of biological polypeptides.^{1–4} Their physical properties resemble those of natural peptides, with some additional traits that make them valuable for pharmaceutical research, including the ability to resist proteases. The folding properties of β - and α/β -peptide oligomers have been thoroughly studied; series of experiments have revealed that these chains can attain regular secondary structures in a side-chain-dependent fashion. We have a good understanding of the principles governing the secondary structure formation at the *ab initio* quantum chemical level.^{5–13} An impressive example is the prediction of the existence of the mixed β -peptide H18/20-helix,⁷ self-association-driven formation of which has been demonstrated experimentally in a chain-length- and solvent-dependent manner.¹⁴ This finding yields the important message that, despite the effective side-chain control, the secondary structure formation is not fully decoupled from the solvent and interchain interactions, and the modeling tools must be honed to handle these effects. Moreover, the modeling of foldameric tertiary and quaternary structure formation,^{2,15} the self-assembly of nanostructures,^{16,17} and foldamer–protein interactions^{18–20} in water explicitly demand validated modeling approaches capable of handling large systems in solvent. Molecular dynamics (MD) simulations have become an indispensable tool for these purposes, and studies concentrating on tuning and validating force fields for the modeling of peptidic chains containing β -amino acids are attracting increasing interest. For the initial sampling of the overall conformational behavior of β -peptidic chains containing both β^2 - and β^3 -side-chains, the CHARMM force field has been utilized together with *ab initio* quantum chemical methods.²¹ It

has also been shown that even unoptimized CHARMM-like parameters with continuum solvent and an explicit water model could be used for the qualitative explanation of many of the experimentally observed behaviors of cyclic-substituted β -peptides.²² The AMBER* force field has been modified in order to produce realistic relative populations of *trans*-dixial and *trans*-diequatorial side-chain orientations of cyclic β -amino acid residues (2-aminocyclopentanecarboxylic acid and 2-aminocyclohexanecarboxylic acid).²³ These MD simulations carried out with the GB/SA chloroform continuum solvation model afforded a qualitative prediction of the helical secondary structures adopted by β -amino acid homo-oligomers. Application of the OPLS-AA force field together with the GB/SA water solvent model²⁴ successfully reflected the experimental trends in the context of β -peptide oligomers designed to fold in aqueous media.²⁵ In a series of seminal publications, thorough quantitative validations against NMR parameters such as 3J couplings and NOE data have been carried out for the GROMOS force field family members in explicit methanol as solvent. In these works, the simulations were successful in reproducing solution-phase NMR observables for peptidic chains constructed from β^3 - and β^2 -amino acids and mixed α/β -peptides.^{26–31} Building on this quantitative validation approach, we aimed to test a force field-explicit water model combination, reportedly tuned to work well together. Such a proven combination is the AMBER force field with the explicit solvent model TIP3P.^{32,33} In this study, we compared the performance of two implementations of the AMBER force field, ff03³⁴ and GAFF (General Amber Force Field),³⁵ for the modeling of β -peptidic chains in water. For the aqueous

Received: June 13, 2014



simulations, three β -peptide sequences were selected, which display basically different folding behavior in water according to the solution-phase experimental characterization (Figure 1).

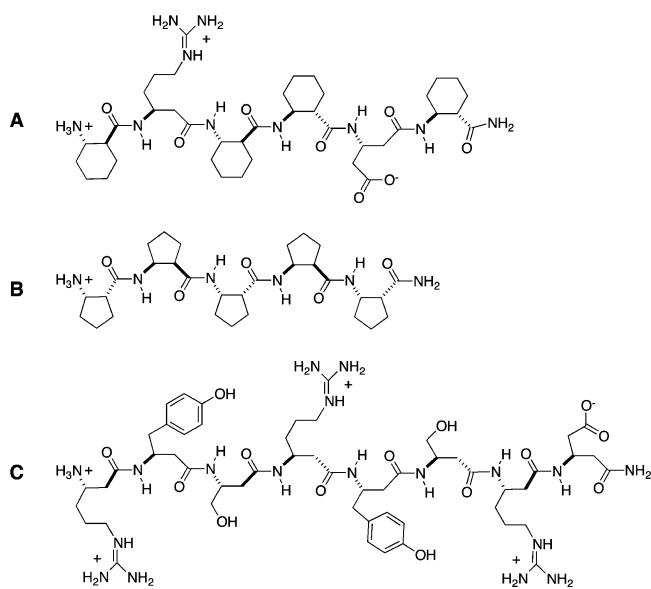


Figure 1. β -Peptidic sequences studied.

Sequence A has been shown to fold into a stable H14 helix in aqueous media, and it serves as a recognition segment for A β oligomers.³⁶ Homologomer B adopts an isolated strand conformation in DMSO,³⁷ and this secondary structure unit self-assembles into nanostructured sheet-mimicking fibers in polar solvents (methanol and water).¹⁷ β -Peptide C is disordered in water (Figures S1 and S2); no long-range contact was observed along the sequence. Here we show that ff03-TIP3P performs well in reproducing NMR spectral parameters for periodic helical and strand-like conformations and predicts disordered behavior, whereas GAFF fails to generate well-ordered conformations.

METHODS

AMBER ff03 is specially tailored toward biopolymers (atom types, bonded and nonbonded parameters available for the constituents of DNA, RNA, and proteins, and some biologically relevant ions), while GAFF is a complete force field covering most of the organic chemical space. These force fields are compatible with each other, and the latter was developed with the intention of facilitating the extension of the force field to arbitrary organic compounds, mainly small organic molecules, such as pharmaceutical ligands. The implementation of the

AMBER force fields in the GROMACS software suite³⁸ employed in our research enabled us to extend the residue-based approach available in ff03 for the proteogenic amino acids to the β -amino acids. The charge assignment was based on *ab initio* calculations at the HF/6-31G* theoretical level, using the RESP fitting method.³⁹ N-Methyl and acetyl capping groups were used on the carboxyl and amino terminals. The quantum chemical calculations were carried out by using the Gaussian09 software package.⁴⁰ RESP fitting was performed on optimized geometries. Residues were parametrized with antechamber⁴¹ and then converted with acpype⁴² to GROMACS topologies. The same charge distribution was used for GAFF and ff03.

The simulations (Table 1) were carried out with explicit solvent in cubic solvation boxes. The TIP3P water model was used in all simulations except B3 and B4, where an equilibrated DMSO solvent box was applied. DMSO was parametrized with GAFF, and the charge distribution was created by using the RESP method. The solvation of the peptides was done with the genbox utility of the GROMACS program suite. Peptides A and B had a net charge of +1, and peptide C had a net charge of +3, which were neutralized by Cl⁻ ions in the system. Simulations with 200 ns time span were run for all sequences, with a step size of 1 fs at 340 K to enhance conformational sampling.^{27,30} Temperature coupling was carried out with a V-rescale algorithm. Neighbor searching was performed at every tenth step. The particle mesh Ewald method was used for electrostatic interactions, with grid-spacing of 0.15 nm. The van der Waals interactions were computed from the neighborhood list with a real space cutoff of 1 nm. Pressure coupling was achieved with the Parinello-Rahman algorithm. Simulations were started from a previously equilibrated solvent box. Simulation of peptide A was performed from two starting structures, a folded H14 helix (A1) and an extended structure (A2), to address the effects of the starting geometry on the simulation.

Backbone atom positional RMSDs were calculated relative to the representative structures of the most populated clusters obtained by clustering trajectories of A1, B1, and C1 after translational superposition of the center of masses, and least-squares rotational fitting of atomic positions along the backbone. Experimental $^3J_{\text{HN-H}\alpha}$ coupling constants were compared with those derived from the ensemble trajectories through the Karplus equation,⁴³ with the coefficients of A = 7.09 Hz, B = -1.42 Hz, and C = 1.55 Hz derived for aqueous solvent.⁴⁴ Histograms of the distributions of the dihedral angles from which the coupling constants were derived were also plotted. The dihedral angles were sorted into 1° bins over the trajectory. Clustering analysis on trajectories was performed to

Table 1. Setup of the Simulations

Sequence	Solvent model	No. of solvent molecules	No. of atoms in peptide	Starting geometry	Force field	Designation
A	TIP3P	3137	127	Helix	ff03	A1
	TIP3P	3254	127	Extended	ff03	A2
	TIP3P	3137	127	Helix	GAFF	A3
B	TIP3P	2254	90	Extended	ff03	B1
	TIP3P	2254	90	Extended	GAFF	B2
	DMSO	985	90	Extended	ff03	B3
C	DMSO	985	90	Extended	GAFF	B4
	TIP3P	3800	182	Helix	ff03	C1
	TIP3P	3800	182	Helix	GAFF	C2

observe the preferred conformational states adopted by the sequences. Clustering was carried out on the backbone atom positional RMSD data with a cutoff of 0.2 nm.²⁶ Clusters with more than 5% of the overall structures were accounted for. Experimentally determined NOE distances were compared with interatomic distances observed in the simulation trajectories. Violation of the upper distance bounds was plotted for the identified NOE interactions.

■ RESULTS AND DISCUSSION

Simulations A1 and A2 tested the ability of the ff03 parameter set to retain the helical structure in water. According to the time evolution of the RMSD values (Figure 2), the lowest

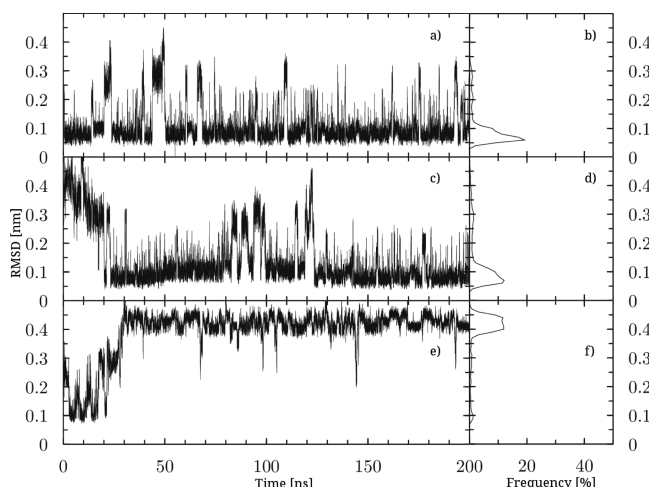


Figure 2. Time evolution and distribution of backbone atom RMSD for simulations A1 (a and b), A2 (c and d), and A3 (e and f). Reference structure was selected from simulation A1 as described in methods.

energy conformation is very close to the starting H14 helix and the sequence remains folded throughout the trajectory. Some partial unfolding events can be observed, which is due to the fraying of the N- and C-termini, but the proximity of the charged side-chains is constant. Starting from the extended structure in simulation A2, we observed folding into the experimentally observed helical conformation within 20 ns. After the folding event, the trajectory resembles that of simulation A1. The folded structure is stable, as indicated by the very small fluctuations in the RMSD. The calculation run with GAFF (A3) displays an RMSD drift in the first 30 ns despite the helical starting conformation. After the rearrangement of the structure, the RMSD remains stable. This indicates that GAFF stabilizes a geometry other than the H14 helix. The

cluster analysis revealed that simulations A1 and A2 resulted in low numbers of clusters (Figures 3 and S3). For A2, clusters capturing not folded intermediate states were slightly more populated due to the folding event. Three major clusters were identified, which contained over 90% of all the structures in the cases of both simulations. The largest cluster in both cases was the folded H14 helix, while the additional low-population clusters represented partially unfolded geometries fraying on either the C- or the N-terminus.

The detailed analysis of the most populated cluster for A3 revealed that GAFF rewound the sequence into a noncompact geometry. The main features were the missing hydrogen bonds stabilizing the H14 helix fold and the contact between the β^3 -hAsp side-chain and the free N-terminal amine. Neither of these was supported by the experimental data (NH/ND exchange, NOE contacts) obtained for sequence A. It is noteworthy that GAFF was unable to produce any folded structure when the calculations were started from the extended geometry.

The experimentally observed NOE distances and $^3J_{\text{HN-H}\alpha}$ values were back-calculated with the trajectories obtained in simulations A1 and A3 (Figure 4). For A1, good agreement was obtained for all the long-range NOEs defining the H14 helix fold (#1–3; for the NOE list, see Table S1). Upper bound violations over 0.05 nm were observed for NOEs NH5 - CaH_4 , NH6 - CaH_5 , and $\text{C}\beta\text{H}_2$ - CaH_2 (#13, 17, and 19). Lower bound violations were not counted, taking into account the nature of the errors associated with the measurement of the NOE interactions. The number of upper bound violations for simulation A3 was significantly higher than that for A1. Importantly, two long-range NOEs out of three were violated. Comparison of the RMSV values of 0.007 and 0.013 nm calculated for A1 and A3, respectively, confirmed that GAFF was less successful in reproducing the experimental NOE data. Back-calculated coupling constants did not display marked deviations from the experimental values, in contrast with the basically different equilibrium fold obtained for A1 and A3. To find a possible explanation, the distributions of the HN-H α dihedral angles were analyzed along the sequence (Figure 5). For A1, the torsions had a monomodal distribution with an average value of 160°, whereas A3 displayed bimodal distributions (maxima at around 160° and 220°) on passing toward the termini. This suggests that the deviation from 180° on both sides may result in relatively high averaged coupling constants, but the actual torsion angles tend to attain unrealistic values, as reflected by the back-calculated NOE data.

Peptide B, designed to mimick the β -strand secondary structure, exhibited strand-like behavior both in DMSO as a stand-alone structure and in water as a building block aggregating into fibers. The combinations of ff03 with TIP3P

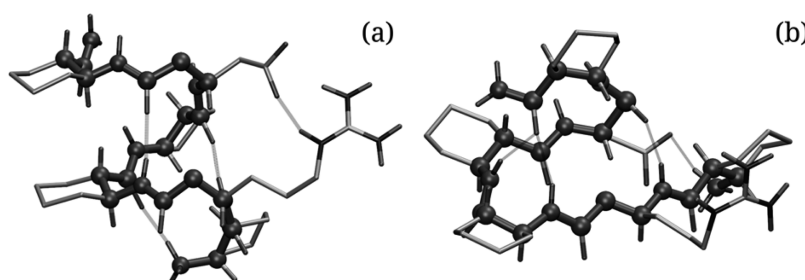


Figure 3. Representative structures of the most populated clusters for simulations A1 (a) and A3 (b).

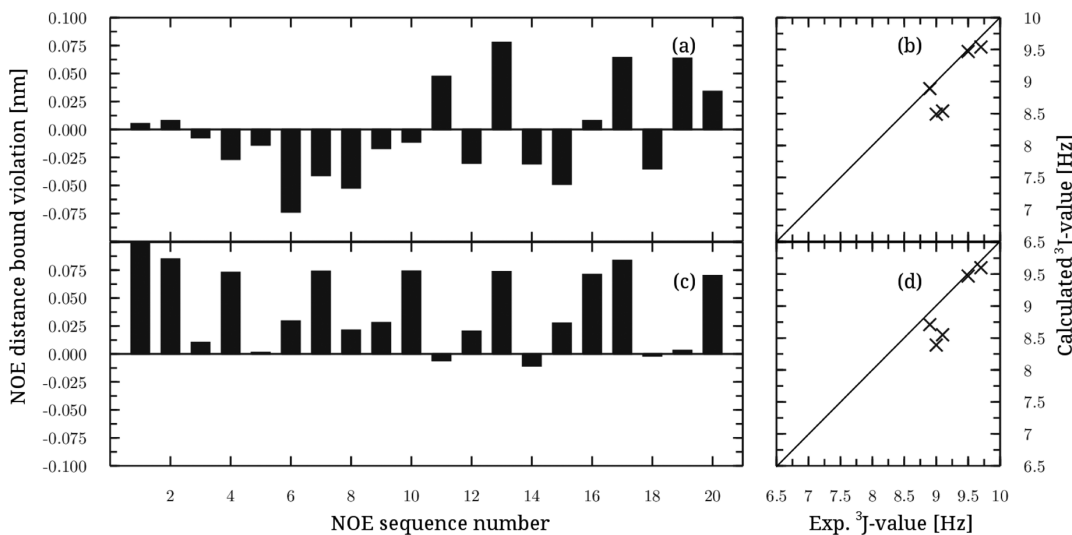


Figure 4. Violation of the NOE bounds by the interatom distances $\langle r^{-6} \rangle^{-1/6}$ averaged over the trajectory and comparison of the back-calculated and measured 3J coupling constants for simulations A1 (a and b) and A3 (c and d). The designations of the NOE interactions are given in Table S1.

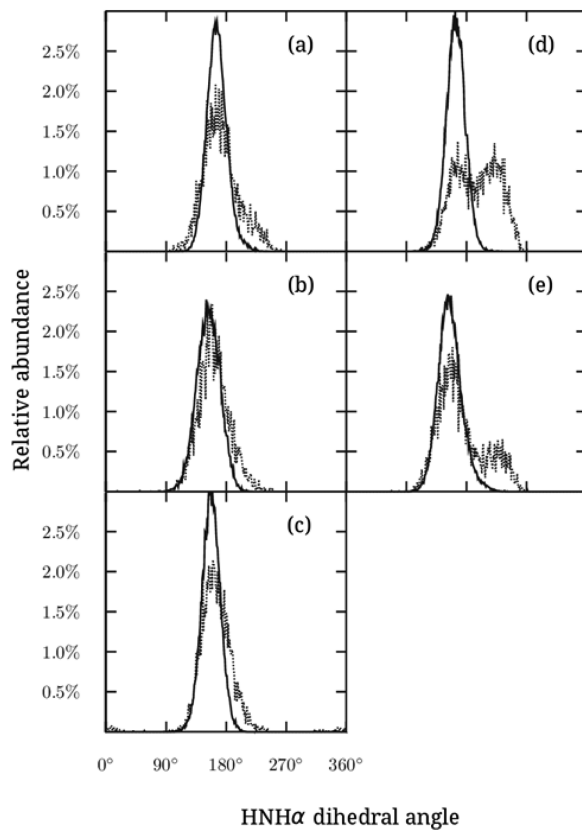


Figure 5. Distribution of the HN–H α dihedral angles over the trajectory for simulations A1 (solid line) and A3 (dashed line). Panels a, b, c, d, and e correspond to residues 2–6, respectively.

and DMSO were tested in simulations B1 and B2. The time evolution of the RMSD indicated (Figure 6) that the simulations converged quickly to equilibrium, and the fluctuations were higher than with those for peptide A. This is acceptable considering the meandering, noncompact nature of the geometry. It was observed experimentally that the structure was more defined in DMSO than in water. Interestingly, GAFF produced lower fluctuations in water than in DMSO.

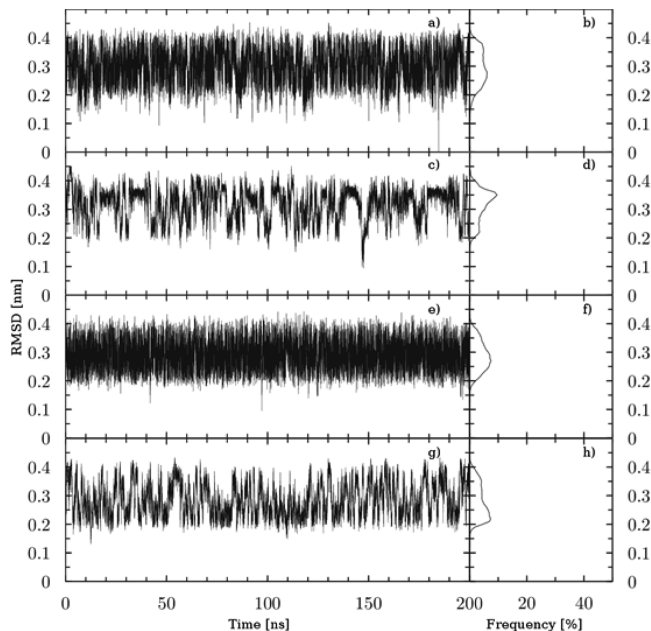


Figure 6. Time evolution and distribution of backbone atom RMSD for simulations B1 (a and b), B2 (c and d), B3 (e and f), and B4 (g and h). The reference structure was selected from simulation B1 as described in the Methods section.

Both the relatively broad RMSD distribution and the cluster analysis (Figure S4) indicated an increased number of conformations in the ensemble. Nevertheless, the eight most populated clusters were found to involve strand geometry (Figure 7), classified as Z6,¹⁰ where the zigzag shaped backbone points the peptide bonds partially toward the solvent in an alternating orientation. This conformation is stabilized by transient local C6 and C8 hydrogen bonds throughout the trajectory.

Comparison of the overall prevailing geometries obtained in simulations B1–B4 did not indicate any difference between the performances of the force fields applied in this case. Back-calculation of the observed NOEs was not helpful either (Figure 8), which was in correlation with the fact that long-range NOEs correlate with the global fold of the structure. All

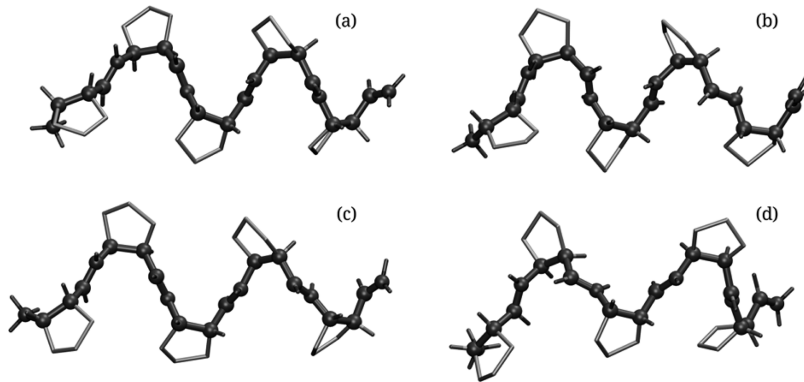


Figure 7. Representative structures of the most populated clusters for simulations B1 (a), B2 (b), B3 (c), and B4 (d).

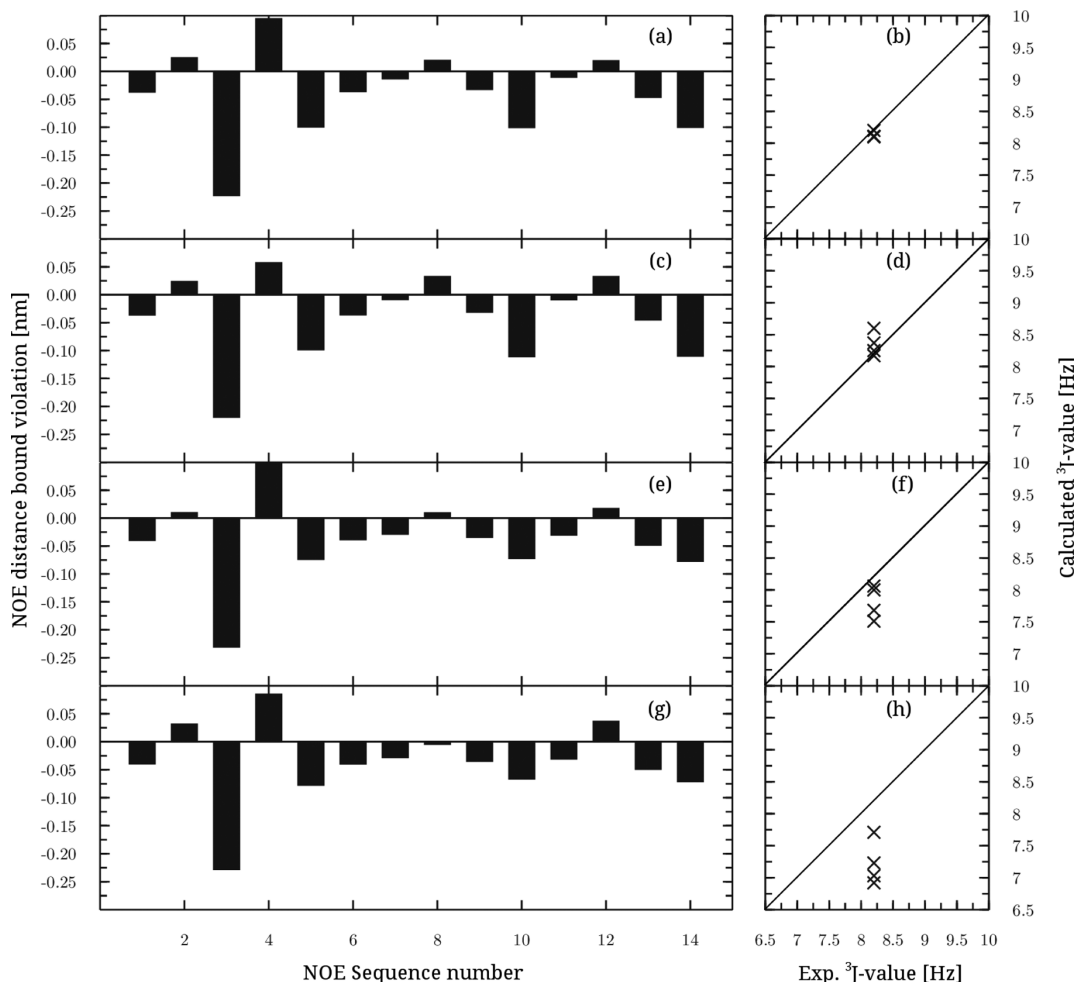


Figure 8. Violation of the NOE bounds by the interatom distances $\langle r^{-6} \rangle^{-1/6}$ averaged over the trajectory and comparison of the back-calculated and measured 3J coupling constants for simulations B1 (a and b), B2 (c and d), B3 (e and f), and B4 (g and h). The designation of the NOE interactions is given in Table S1.

the simulations produced very few upper bound violations, with only one difference above 0.05 nm. The RSMVs were calculated as 0.007, 0.005, 0.008, and 0.007 nm for simulations B1–B4, respectively. It must be noted that experimental NOEs were obtained in DMSO, but the simulations did not reveal any difference from the behavior in water for the isolated strand. The back-calculated $^3J_{\text{HN-H}\alpha}$ values, on the other hand, were perceptibly different from the experimental values. GAFF did

not reproduce the coupling constants faithfully, whereas ff03 yielded good agreement.

Since simulations A1–A3 indicated the basic differences in the HN–H α dihedral angle preferences of the force fields ff03 and GAFF, we again suspected the different torsion tuning to explain the better performance of ff03 in reproducing backbone coupling constants. Distribution analysis revealed (Figure 9) that ff03 was less prone to generate bimodal distribution, and the most populated region was at around 180°. This

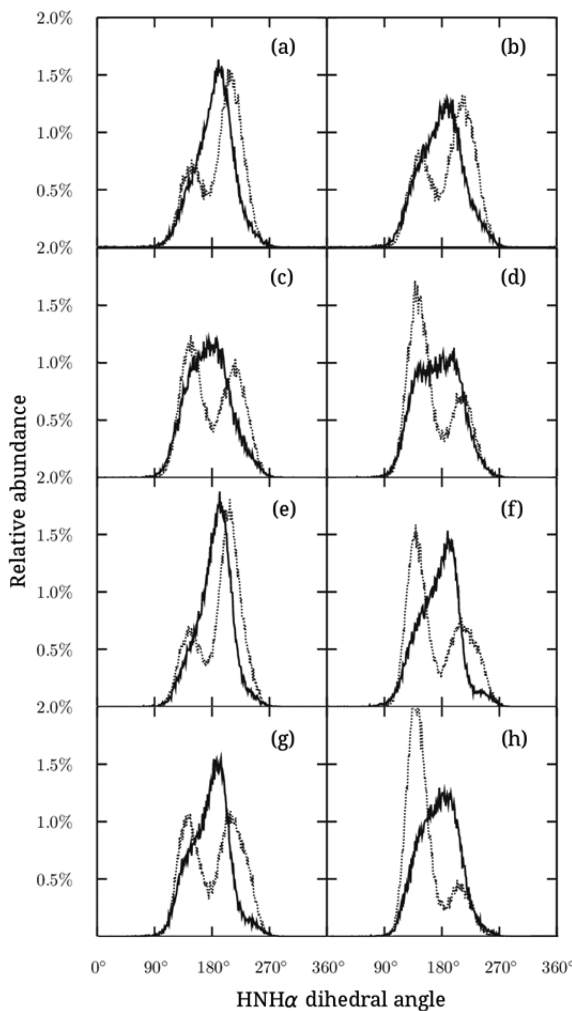


Figure 9. Distribution of the HN–H α dihedral angles over the trajectory for simulations carried out with ff03 (solid lines) and GAFF (dashed lines). Panels a–d represent results from simulation B2 for residues 2–5, respectively. Panels e–h represent results from simulation B4 for residues 2–5, respectively.

arrangement is able to produce larger 3J couplings, and therefore, ff03 approximated the experimental values better. The potential energy surface scan that we carried out for the dihedrals HN–H α and CO–H β at the *ab initio* theoretical level of MP2/cc-PVTZ (Figure S5) supported the monomodal distribution for torsion HN–H α in the *cis*-2-amino cyclohexane acid building block of peptide B. The dihedral terms in GAFF are described via the Ryckaert–Belleman potentials with 1–4 Lennard-Jones (L-J) interactions switched off. For ff03, dihedral contributions are calculated by using sum of periodic functions in combination with specially tuned 1–4 L-J potentials. In this work, other vdW parameters and charge distributions were identical for both GAFF and ff03. This setup suggests that the different dihedral angle distributions are due to the combined effects of the functional form, the parameters, and the handling of the 1–4 vdW interactions.

The force field ff03 has been developed to model the structure formation behavior of natural peptides/proteins. On the other hand, the prediction of disorder is equally important when rational design comes into the picture. β -Peptide foldamers built up from β^3 -amino acid residues tend to form an H14 helix, stabilization of which in water is possible by

placing complementary charged side-chains in positions *i* to *i* + 3.²⁵ It is plausible that this propensity can be overridden by using identical charges on one face of the H14 helix. Peptide C was therefore designed to be disordered in water with the *i* to *i* + 3 β^3 -hArg pattern. Accordingly, low signal dispersion and no long-range interaction were detected in NMR, indicating the absence of any predominant compact and periodic conformation (Figures S1 and S2). The time evolution curves of the RMSD values for simulations C1–C2 clearly reflected this behavior. Large fluctuations were observed as compared with the results for simulations A1–A3 and B1–B4 (Figure 10). The

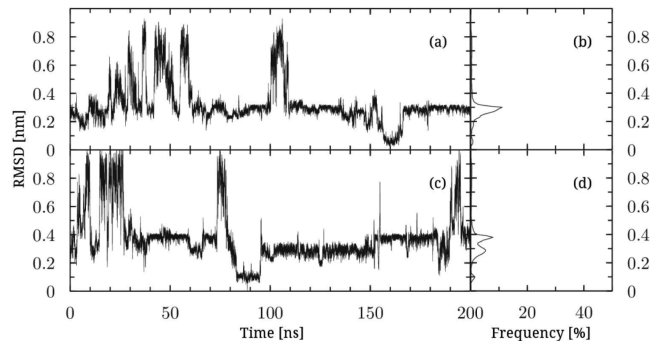


Figure 10. Time evolution and distribution of backbone atom RMSD for simulations C1 (a and b) and C2 (c and d). The reference structure was selected from simulation C1 as described in the Methods section.

structure cannot fully converge to a stable compact equilibrium geometry. The cluster analysis revealed that conformations maximizing the distance between the β^3 -hArg side-chains prevail and these are not specific periodic secondary structures (Figure S6). The residue distance matrix averaged over the 200 ns trajectory did not reveal any tendency of preferential contacts between nonsequential residues (Figure S7).

To address the effect of the solvent, simulations A1, A2, and B1 were repeated without the TIP3P explicit solvent. The absence of the solvent caused marked differences in the folding process and structures. For peptide A, the simulation with the helical initial coordinates was trapped in the starting conformation (Figure S8). Starting from an elongated conformation, peptide A did not adopt the expected helix; there was no folding process (Figure S9). In the case of peptide B (Figure S10), the elongated starting structure converged to bent conformations, which were stabilized by contacts between the charged N-terminus and the amide oxygens of the backbone (Figure S11). These results strongly suggested that the explicit solvent model is essential to properly capture the folding processes of the β -peptides studied.

CONCLUSIONS

Through the use of AMBER ff03 and GAFF parameters and RESP charges, MD simulations were run in explicit solvents, including water and DMSO for β -peptides. The sequences were selected to cover diverse conformational behavior: compact helix, strand mimetic geometry, and the state of disorder, which was achieved by means of a combination of stereochemical programming of the backbone geometry and changing the charge pattern of the side-chains. It was found that GAFF was not able to predict folding for the helical sequence. Accordingly, the back-calculation of the NMR spectral parameters was not successful and this was also apparent for the Z6-strand mimetic.

The failure of GAFF to produce realistic conformation ensembles could be explained (at least in part) by its biased torsional preferences along the peptide backbone, leading to bimodal distribution of the corresponding torsion angles. Our simulations run with ff03 were able to reproduce the compact H14 helical fold of peptide A and the stereochemically stabilized Z6-strand propensity of peptide B without experimental restraints. The back-calculated NOE and 3J coupling data were in acceptable agreement with the experimental findings. In this work, we made an attempt to validate the force field combination against a β -peptidic sequence displaying a Coulomb repulsion-driven disorder. The random conformational ensemble was successfully predicted by the simulations, and we could therefore conclude that the ff03-TIP3P parameters did not exhibit bias toward the folded states for the β -peptidic foldamers. The quantitative validation approach allowed the conclusion that the prediction performance in aqueous medium of the ff03-TIP3P force field combination was comparable with that obtained for the GROMOS force field family in explicit methanol.^{26–31} Comparison with other force fields (CHARMM and OPLS-AA) will require a similar validation methodology for β -peptides including explicit solvent model and NMR data.

In possession of these results, we can suggest ff03-TIP3P for MD simulations of biomimetic sequences containing β -amino acid residues. The modular implementation of this biomolecule-compatible force field and the explicit water model will allow the simulation of protein-sized foldameric systems, protein–foldamer interactions, or chimera structures constructed via protein prosthesis in an aqueous environment.

ASSOCIATED CONTENT

Supporting Information

Experimental NOE data taken from the literature for peptides A and B, HPLC, MS, and NMR characterization data for sequence C, results of cluster analyses, *ab initio* potential energy surface, and residue distance matrix. This material is available free of charge via the Internet at <http://pubs.acs.org>.

AUTHOR INFORMATION

Corresponding Author

*Institute of Pharmaceutical Analysis. E-mail: martinek@pharm.u-szeged.hu. Phone: +36303371820.

Author Contributions

The manuscript was written through contributions of all the authors. All the authors have given approval to the final version of the manuscript.

Funding

This work was supported by the Hungarian Research Foundation (OTKA K83882) and the Hungarian Academy of Sciences, Lendület program (LP-2011-009). Computations were carried out at the HPC Center of the University of Szeged (TAMOP-4.2.2.C-11/1/KONV-2012-0010).

Notes

The authors declare no competing financial interest.

ABBREVIATIONS

DMSO, dimethyl sulfoxide; RESP, restrained electrostatic potential; RMSD, root-mean-square deviation; MD, molecular dynamics

REFERENCES

- (1) Cheng, R. P.; Gellman, S. H.; DeGrado, W. F. Beta-Peptides: From Structure to Function. *Chem. Rev.* **2001**, *101*, 3219–3232.
- (2) Johnson, L. M.; Gellman, S. H. Alpha-Helix Mimicry with alpha/beta-Peptides. *Methods Enzymol.* **2013**, *523*, 407–429.
- (3) Martinek, T. A.; Fulop, F. Peptidic Foldamers: Ramping up Diversity. *Chem. Soc. Rev.* **2012**, *41*, 687–702.
- (4) Seebach, D.; Matthews, J. L. Beta-Peptides: A Surprise at Every Turn. *Chem. Commun.* **1997**, 2015–2022.
- (5) Beke, T.; Somlai, C.; Perczel, A. Toward a Rational Design of beta-Peptide Structures. *J. Comput. Chem.* **2006**, *27*, 20–38.
- (6) Baldauf, C.; Gunther, R.; Hofmann, H. J. Theoretical Prediction of the Basic Helix Types in alpha,beta-Hybrid Peptides. *Biopolymers* **2006**, *84*, 408–413.
- (7) Baldauf, C.; Gunther, R.; Hofmann, H. J. Mixed Helices—A General Folding Pattern in Homologous Peptides? *Angew. Chem., Int. Ed.* **2004**, *43*, 1594–1597.
- (8) Baldauf, C.; Gunther, R.; Hofmann, H. J. Side-chain Control of Folding of the Homologous alpha-, beta-, and gamma-Peptides into "mixed" helices (beta-helices). *Biopolymers* **2005**, *80*, 675–87.
- (9) Pohl, G.; Beke-Somfai, T.; Csizmadia, I. G.; Perczel, A. Exploiting Diverse Stereochemistry of beta-Amino Acids: Toward a Rational Design of Sheet-Forming beta-Peptide Systems. *Amino Acids* **2012**, *43*, 735–49.
- (10) Beke, T.; Csizmadia, I. G.; Perczel, A. On the Flexibility of beta-Peptides. *J. Comput. Chem.* **2004**, *25*, 285–307.
- (11) Pohl, G.; Beke, T.; Csizmadia, I. G.; Perczel, A. Extended Apolar beta-Peptide Foldamers: the Role of Axis Chirality on beta-Peptide Sheet Stability. *J. Phys. Chem. B* **2010**, *114*, 9338–9348.
- (12) Sharma, G. V. M.; Chandramouli, N.; Choudhary, M.; Nagendar, P.; Ramakrishna, K. V. S.; Kunwar, A. C.; Schramm, P.; Hofmann, H. J. Hybrid Helices: Motifs for Secondary Structure Scaffolds in Foldamers. *J. Am. Chem. Soc.* **2009**, *131*, 17335–17344.
- (13) Baldauf, C.; Hofmann, H. J. Ab Initio MO Theory—An Important Tool in Foldamer Research: Prediction of Helices in Oligomers of omega-Amino Acids. *Helv. Chim. Acta* **2012**, *95*, 2348–2383.
- (14) Szolnoki, E.; Hetenyi, A.; Mandity, I. M.; Fulop, F.; Martinek, T. A. Foldameric beta-H18/20(P) Mixed Helix Stabilized by Head-to-Tail Contacts: A Way to Higher-Order Structures. *Eur. J. Org. Chem.* **2013**, 3555–3559.
- (15) Wang, P. S.; Nguyen, J. B.; Schepartz, A. Design and High-Resolution Structure of a beta(3)-Peptide Bundle Catalyst. *J. Am. Chem. Soc.* **2014**, *136*, 6810–6813.
- (16) Torres, E.; Gorrea, E.; Burusco, K. K.; Da Silva, E.; Nolis, P.; Rua, F.; Boussert, S.; Diez-Perez, I.; Dannenberg, S.; Izquierdo, S.; Giralt, E.; Jaime, C.; Branchadell, V.; Ortuno, R. M. Folding and Self-Assembling with beta-Oligomers Based on (1R,2S)-2-Aminocyclobutane-1-carboxylic acid. *Org. Biomol. Chem.* **2010**, *8*, 564–575.
- (17) Martinek, T. A.; Hetenyi, A.; Fulop, L.; Mandity, I. M.; Toth, G. K.; Dekany, I.; Fulop, F. Secondary Structure Dependent Self-Assembly of Beta-Peptides into Nanosized Fibrils and Membranes. *Angew. Chem., Int. Ed.* **2006**, *45*, 2396–2400.
- (18) Haase, H. S.; Peterson-Kaufman, K. J.; Lan Levengood, S. K.; Checco, J. W.; Murphy, W. L.; Gellman, S. H. Extending Foldamer Design Beyond alpha-Helix Mimicry: alpha/beta-Peptide Inhibitors of Vascular Endothelial Growth Factor Signaling. *J. Am. Chem. Soc.* **2012**, *134*, 7652–7655.
- (19) Harker, E. A.; Schepartz, A. Cell-Permeable beta-Peptide Inhibitors of p53/Hdm2 Complexation. *ChemBioChem* **2009**, *10*, 990–993.
- (20) Shandler, S. J.; Korendovych, I. V.; Moore, D. T.; Smith-Dupont, K. B.; Streu, C. N.; Litvinov, R. I.; Billings, P. C.; Gai, F.; Bennett, J. S.; DeGrado, W. F. Computational Design of a beta-Peptide that Targets Transmembrane Helices. *J. Am. Chem. Soc.* **2011**, *133*, 12378–12381.
- (21) Mohle, K.; Gunther, R.; Thormann, M.; Sewald, N.; Hofmann, H. J. Basic Conformers in beta-Peptides. *Biopolymers* **1999**, *50*, 167–184.

- (22) Rathore, N.; Gellman, S. H.; de Pablo, J. J. Thermodynamic Stability of beta-Peptide Helices and the Role of Cyclic Residues. *Biophys. J.* **2006**, *91*, 3425–3435.
- (23) Christianson, L. A.; Lucero, M. J.; Appella, D. H.; Klein, D. A.; Gellman, S. H. Improved Treatment of Cyclic beta-Amino Acids and Successful Prediction of beta-Peptide Secondary Structure Using a Modified Force Field: AMBER**C*. *J. Comput. Chem.* **2000**, *21*, 763–773.
- (24) Chandrasekhar, J.; Saunders, M.; Jorgensen, W. L. Efficient Exploration of Conformational Space Using the Stochastic Search Method: Application to beta-Peptide Oligomers. *J. Comput. Chem.* **2001**, *22*, 1646–1654.
- (25) Kritzer, J. A.; Tirado-Rives, J.; Hart, S. A.; Lear, J. D.; Jorgensen, W. L.; Schepartz, A. Relationship Between Side Chain Structure and 14-Helix Stability of beta(3)-Peptides in Water. *J. Am. Chem. Soc.* **2005**, *127*, 167–178.
- (26) Daura, X.; Gademann, K.; Jaun, B.; Seebach, D.; van Gunsteren, W. F.; Mark, A. E. Peptide Folding: When Simulation Meets Experiment. *Angew. Chem., Int. Ed.* **1999**, *38*, 236–240.
- (27) Zagrovic, B.; Gattin, Z.; Lau, J.-C.; Huber, M.; Gunsteren, W. Structure and Dynamics of Two beta-Peptides in Solution from Molecular Dynamics Simulations Validated against Experiment. *Eur. Biophys. J.* **2008**, *37*, 903–912.
- (28) Niggli, D. A.; Ebert, M. O.; Lin, Z.; Seebach, D.; van Gunsteren, W. F. Helical Content of a beta(3)-Octapeptide in Methanol: Molecular Dynamics Simulations Explain a Seeming Discrepancy Between Conclusions Derived from CD and NMR Data. *Chem.—Eur. J.* **2012**, *18*, 586–593.
- (29) Wang, D. Q.; Freitag, F.; Gattin, Z.; Haberkern, H.; Jaun, B.; Siwko, M.; Vyas, R.; van Gunsteren, W. F.; Dolenc, J. Validation of the GROMOS 54A7 Force Field Regarding Mixed alpha/beta-Peptide Molecules. *Helv. Chim. Acta* **2012**, *95*, 2562–2577.
- (30) Huang, W.; Lin, Z.; van Gunsteren, W. F. Validation of the GROMOS 54A7 Force Field with Respect to beta-Peptide Folding. *J. Chem. Theory Comput.* **2011**, *7*, 1237–1243.
- (31) Lin, Z.; van Gunsteren, W. F. Refinement of the Application of the GROMOS 54A7 Force Field to beta-Peptides. *J. Comput. Chem.* **2013**, *34*, 2796–805.
- (32) Mackerell, A. D., Jr. Empirical Force Fields for Biological Macromolecules: Overview and Issues. *J. Comput. Chem.* **2004**, *25*, 1584–1604.
- (33) Paschek, D.; Day, R.; Garcia, A. E. Influence of Water-Protein Hydrogen Bonding on the Stability of Trp-Cage Miniprotein. A Comparison Between the TIP3P and TIP4P-Ew Water Models. *Phys. Chem. Chem. Phys.* **2011**, *13*, 19840–19847.
- (34) Duan, Y.; Wu, C.; Chowdhury, S.; Lee, M. C.; Xiong, G.; Zhang, W.; Yang, R.; Cieplak, P.; Luo, R.; Lee, T.; Caldwell, J.; Wang, J.; Kollman, P. A Point-Charge Force Field for Molecular Mechanics Simulations of Proteins Based on Condensed-Phase Quantum Mechanical Calculations. *J. Comput. Chem.* **2003**, *24*, 1999–2012.
- (35) Wang, J.; Wolf, R. M.; Caldwell, J. W.; Kollman, P. A.; Case, D. A. Development and Testing of a General Amber Force Field. *J. Comput. Chem.* **2004**, *25*, 1157–1174.
- (36) Fulop, L.; Mandity, I. M.; Juhasz, G.; Szegedi, V.; Hetenyi, A.; Weber, E.; Bozso, Z.; Simon, D.; Benko, R.; Kiraly, Z.; Martinek, T. A. A Foldamer-Dendrimer Conjugate Neutralizes Synaptotoxic beta-Amyloid Oligomers. *PLoS One* **2012**, *7*, e39485.
- (37) Martinek, T. A.; Toth, G. K.; Vass, E.; Hollosi, M.; Fulop, F. *cis*-2-Aminocyclopentanecarboxylic Acid Oligomers Adopt a Sheetlike Structure: Switch from Helix to Nonpolar Strand. *Angew. Chem., Int. Ed.* **2002**, *41*, 1718–1721.
- (38) Van Der Spoel, D.; Lindahl, E.; Hess, B.; Groenhof, G.; Mark, A. E.; Berendsen, H. J. C. GROMACS: Fast, Flexible, and Free. *J. Comput. Chem.* **2005**, *26*, 1701–1718.
- (39) Bayly, C. I.; Cieplak, P.; Cornell, W. D.; Kollman, P. A.; Well-Behaved, A. Electrostatic Potential Based Method Using Charge Restraints for Deriving Atomic Charges —The Resp Model. *J. Phys. Chem.* **1993**, *97*, 10269–10280.
- (40) Frisch, M. J.; Trucks, G. W.; Schlegel, H. B.; Scuseria, G. E.; Robb, M. A.; Cheeseman, J. R.; Scalmani, G.; Barone, V.; Mennucci, B.; Petersson, G. A.; Nakatsuji, H.; Caricato, M.; Li, X.; Hratchian, H. P.; Izmaylov, A. F.; Bloino, J.; Zheng, G.; Sonnenberg, J. L.; Hada, M.; Ehara, M.; Toyota, K.; Fukuda, R.; Hasegawa, J.; Ishida, M.; Nakajima, T.; Honda, Y.; Kitao, O.; Nakai, H.; Vreven, T.; Montgomery, J. A.; Jr., Peralta, J. E.; Ogliaro, F.; Bearpark, M.; Heyd, J. J.; Brothers, E.; Kudin, K. N.; Staroverov, V. N.; Kobayashi, R.; Normand, J.; Raghavachari, K.; Rendell, A.; Burant, J. C.; Iyengar, S. S.; Tomasi, J.; Cossi, M.; Rega, N.; Millam, J. M.; Klene, M.; Knox, J. E.; Cross, J. B.; Bakken, V.; Adamo, C.; Jaramillo, J.; Gomperts, R.; Stratmann, R. E.; Yazyev, O.; Austin, A. J.; Cammi, R.; Pomelli, C.; Ochterski, J. W.; Martin, R. L.; Morokuma, K.; Zakrzewski, V. G.; Voth, G. A.; Salvador, P.; Dannenberg, J. J.; Dapprich, S.; Daniels, A. D.; Ö. Farkas, Foresman, J. B.; Ortiz, J. V.; Cioslowski, J.; , and Fox, D. J., *Gaussian 09*, Revision D.01; Gaussian, Inc.: Wallingford, CT, 2009.
- (41) Wang, J.; Wang, W.; Kollman, P. A.; Case, D. A. Automatic Atom Type and Bond Type Perception in Molecular Mechanical Calculations. *J. Mol. Graph. Model.* **2006**, *25*, 247–260.
- (42) Sousa da Silva, A.; Vranken, W. ACPYPE—AnteChamber PYthon Parser interfacE. *BMC Res. Notes* **2012**, *5*, 367–375.
- (43) Karplus, M.; Anderson, D. H. Valence-Bond Interpretation of Electron-Coupled Nuclear Spin Interactions; Application to Methane. *J. Chem. Phys.* **1959**, *30*, 6–10.
- (44) Hu, J. S.; Bax, A. Determination of phi and chi(1) Angles in Proteins from C-13-C-13 Three-Bond J Couplings Measured by Three-Dimensional Heteronuclear NMR. How Planar is the Peptide Bond? *J. Am. Chem. Soc.* **1997**, *119*, 6360–6368.